ADVANCED FUNCTIONAL MATERIALS
www.afm-journal.de

SnO_2-C_{60} Pyrrolidine Tris-Acid (CPTA) as the Electron Transport Layer for Highly Efficient and Stable Planar Sn-Based Perovskite Solar Cells

Zijiang Yang, Meiyan Zhong, Yongqi Liang, Liangwei Yang, Xingyi Liu, Qi Li, Jin Zhang, and Dongsheng Xu**

For solar cell applications, Sn-based hybrid perovskites have drawn particular interest due to their environmental friendliness. Here, a thin layer of C_{60} pyrrolidine tris-acid (CPTA) is found essential for achieving high efficiency with planar solar cells of Sn-based perovskites. As a result, a power conversion efficiency of 7.40% is achieved for {en}$FASnI_3$ solar cells with a planar n–i–p architecture, and the device exhibits excellent stability in air. For the first time, highly efficient Sn-based hybrid perovskite solar cells on n–i–p architecture are achieved. A V_{oc} of 0.72 V is highlighted as the highest V_{oc} ever reported for $FASnI_3$ solar cells.

1. Introduction

In the past decade, Pb-based hybrid perovskite solar cells (PSCs) have achieved an impressive (up to 24.2%) power conversion efficiency (PCE).[1,2] Despite these significant progresses, the toxicity of lead limits the large-scale application of PSCs.[3] Soon after the development of Pb-based perovskites, researchers start to replace the toxic Pb due to the environmental concerns.[4,5] Sn is an attractive alternative because Sn-based perovskite has similar optical and electronic properties comparing with Pb-based perovskite.[6] However, research in this direction is hindered by the poor stability of the Sn-based perovskite in the air.[7] One of most probable reasons is reported to be the oxidation of Sn^{2+} to Sn^{4+}.[8] The oxidation process[9] will heavily dope the perovskites and make them behave like a metallic conductor. This in turn will cause excessive carrier recombination and sometimes even short-circuit the devices. Several strategies have been developed to protect the Sn-based perovskite, such as the adding of SnF_2,[10] controlling the reducing atmosphere,[11] the forming of 2D/3D composite[12,13]or 3D hollow structures.[14–17] In order to achieve higher efficiency and stability, Sn-based perovskite have relied on mesoporous TiO_2 as the electron-selective layer.[18,19] The introduction of mesoporous TiO_2 makes manufacture process more complex, and the high-temperature needed for processing hampers the development of perovskite-based monolithic tandem devices and flexible wearable solar cells.[20,21] In contrast, the simplicity of the planar heterojunction indicates that a planar architecture is more technically feasible.[22] Besides, planar PSCs can be fabricated via solution processing at low temperatures (<150 °C), thus greatly reducing manufacturing costs. However, compared to the mesoporous-type PSC, its planar-type counterpart suffers from very low PCE,[23,24] probably due to the poor contact of the interfaces[25] and unsuitable charge transporting layer.[23]

Here, we tried SnO_2 as the electron transport layer to fabricate a n–i–p planar-architecture, but was not successful. Then we introduced a hydrophilic derivative of fullerene, namely, the C_{60} pyrrolidine tris-acid (CPTA) between SnO_2 and the perovskite. As a result, we achieved a power conversion efficiency above 7.40% for Sn-based perovskite devices with the planar architecture. This shows that not only mesoporous-architecture devices, but also n–i–p planar-architecture devices can be highly efficient in the Sn-based PSCs. Thanks to the CPTA layer in our planar Sn-based PSCs, we attained a V_{oc} of 0.72 V, which represents the highest value ever reported for $FASnI_3$ solar cells.

2. Results and Discussion

We fabricated Sn-based PSCs with the planar n–i–p architecture (**Figure 1**a). A SnO_2 compact layer deposited on the fluorine-doped tin oxide (FTO) substrate was employed as an electron transport layer. C_{60} pyrrolidine tris-acid (CPTA) was then deposited onto the SnO_2-covered FTO substrate. Figure 1b shows the X-ray diffraction (XRD) pattern of the {en}$FASnI_3$ films. The peaks of FTO substrate are marked with black dots. The {en}$FASnI_3$ films exhibit a shift of the Bragg reflections to

Dr. Z. Yang, M. Zhong, Prof. Y. Liang, X. Liu, Prof. Q. Li, Prof. D. Xu
Beijing National Laboratory for Molecular Sciences
State Key Laboratory for Structural Chemistry of Unstable and Stable Species
College of Chemistry and Molecular Engineering
Peking University
100871 Beijing, China
E-mail: yongqi.liang@pku.edu.cn; dsxu@pku.edu.cn
Dr. L. Yang, Prof. J. Zhang
Center for Nanochemistry
Beijing Science and Engineering Center for Nanocarbons
Peking University
100871 Beijing, China
The ORCID identification number(s) for the author(s) of this article can be found under https://doi.org/10.1002/adfm.201903621.

DOI: 10.1002/adfm.201903621

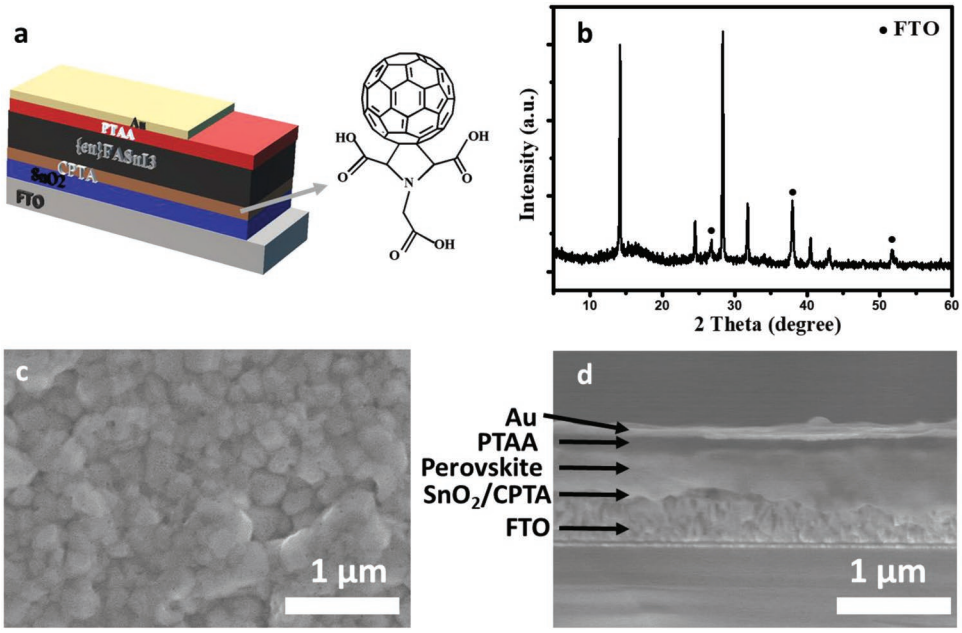

Figure 1. a) Schematic illustration of the device architecture and the molecular structure of CPTA. b) XRD pattern of the {en}$FASnI_3$ film. The diffraction peaks from the FTO substrate are marked with black dots. c) SEM morphological image of the {en}$FASnI_3$ film. ({en}$FASnI_3$ is a 3D hollow perovskite, which was first reported by Kanatzidis et al.[15] Ethylenediammonium is abbreviated as en.) The grain size of {en}$FASnI_3$ is ≈200–300 nm. d) Cross-sectional SEM image of a complete solar cell. The perovskite layer is about 400 nm.

smaller 2θ angles compared with the $FASnI_3$ film (Figure S1a, Supporting Information). The decrease of the 2θ angles indicates the increase of unit cell volume, thus confirming the existence of {en}$FASnI_3$.[15] Moreover, the proton nuclear magnetic resonance (^{1}H-NMR) Spectrum and UV–vis spectra also confirm the presence of ethylenediamine in perovskite thin films (Figure S1b,c, Supporting Information). Scanning electron microscopy (SEM) was used to characterize the morphology of the {en}$FASnI_3$ films Figure 1c. Similar to previous reports,[16] the grain size of the {en}$FASnI_3$ film is obviously smaller than the $FASnI_3$ film (Figure S2, Supporting Information). We note that the Sn-based perovskite were usually fabricated by one-step method[26] and two-step method,[27,28] while the antisolvent assisted one-step method was rarely adopted.[29] As Sn-based perovskites might crystallize faster than Pb-based perovskite materials, it is more difficult to control crystallization by means of commonly used antisolvents.[17,30] The choice of antisolvent is found to be critical for high-quality films, and films prepared with chloroform as an antisolvent show the best quality (Figure S3, Supporting Information). While the exact reason is still unknown, we propose that the unique role of chloroform might be related to the hydrogen bonding formation.[31] From the cross-sectional SEM image (Figure 1d), it can be observed that the perovskite layer is ≈400 nm thick, and the PTAA layer is about 100 nm thick. Though it has been predicted the carrier diffusion length in Sn perovskite can be over 500 nm from ultrafast spectroscopy characterization,[32] efficient planar devices with Sn-based perovskite films have not been reported. Instead, mesoporous devices have to be made so that the electron diffusion can be facilitated via the mesoporous TiO_2 scaffold.[17,32,33] Here, the photovoltaic performance shown below for the {en}$FASnI_3$ films of 400 nm thickness represents a direct proof that the electron diffusion length can be high for Sn-based perovskites.

Figure 2a shows the Raman spectrum of the CPTA film, which is deposited on the FTO/ SnO_2 substrate. The Raman peaks at ≈600 and 1100 cm^{-1} are due to SnO_2 film.[34] The peaks at 1459 and 1564 cm^{-1} can be assigned to the vibrations of C_{60} rings, which is consistent with the peak of CPTA powder (blue line). This confirms the existence of the CPTA layer on the SnO_2. Moreover, in order to investigate the interaction between SnO_2 and CPTA, X-ray photoelectron spectroscopy (XPS) is carried out (Figure 2b). The photoelectron binding energy of SnO_2-CPTA film at Sn 3d level is slightly higher than that of SnO_2 film, which indicates that there is additional negative charge around the Sn atoms. As an electron donor, CPTA coordinates with Sn atoms in SnO_2 to form Lewis adducts. In order to measure the thickness of CPTA functional layer, we conducted tapping-mode atomic force microscopy (AFM) to observe the steps of SnO_2 and SnO_2-CPTA. The thickness of step is about 18 nm, which is the thickness of CPTA layer (Figure S4, Supporting Information).

We then studied the photovoltaic performance of the PSCs. The solar cell used the SnO_2 without modification of CPTA as electron transport layer shows very low efficiency. This indicates that CPTA is very important for the construction of n–i–p Sn-based PSCs. (**Figure 3**a). In contrast, the solar cell with SnO_2-CPTA electron transport layer achieved a PCE of 6.54%. Especially, The V_{OC} is up to 0.722 V (forward scan). Previously, the highest V_{OC} achieved for $FASnI_3$ solar cells is 0.42 and 0.47 V for normal/mesoporous and inverted architecture, respectively. The highest V_{OC} achieved for hollow $FASnI_3$ solar cells is 0.48 V. We have to mention that the highest for $MASnI_3$ is 0.88 V,[5] approaching its own theoretical limit. However,

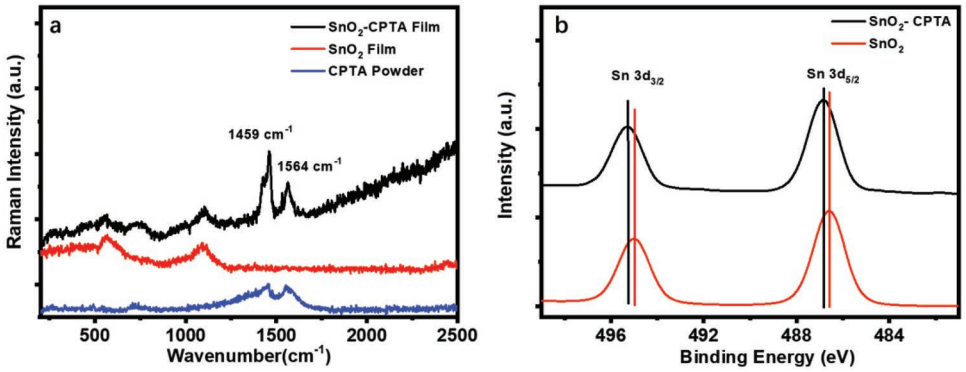

Figure 2. a) Raman spectrum of the FTO-SnO_2 films with/without CPTA layer. Black line, SnO_2-CPTA film; red line, SnO_2 film; blue line, CPTA powder. b) X-ray photoelectron spectroscopy (XPS) of the FTO-SnO_2 films with/without CPTA layer at Sn 3d level.

poor reproducibility is definitely noted. We believe that the leap forward from 0.48 to 0.72 V here represents a breakthrough in the field. Figure 3b shows the *J–V* curves under simulated AM1.5 sunlight for the champion solar cell (relative humidity = 60%, RT = 25 °C), measured under reverse and forward voltage scans. The solar cell achieved a PCE of 7.40%, with a high open circuit voltage (V_{OC}) of 0.687 V, a short-circuit current density (J_{SC}) of 16.45 mA cm^{-2}, and a fill factor (FF) of 0.65 when measured under a forward scan. At the same time, the solar cell achieved a PCE of 5.03%, with an open circuit voltage (V_{OC}) of 0.525 V, a short-circuit current density (J_{SC}) of 16.45 mA cm^{-2}, and a fill factor (FF) of 0.58 when measured under a reverse scan. It is worth noting that there exists significant inverted-hysteresis when the solar cell is scanned in the two directions. However, as is clearly found (also mentioned in $FASnI_3$ solar cells of inverted architecture,[35] but to much less degree) the trend is inverted here. We try to study how the hysteresis and *J–V* performance could be affected by the scan speed (Figure S5 and Table S1, Supporting Information). However, for now, we cannot explain this phenomenon in the Sn-based PSCs for the time being, but it is very probable that the timescale difference between ionic migration and electron transport inside the device might account for the finding here.[36,37] Figure 3c shows the stabilized photocurrent output of the solar cell under bias of 0.435 V. The photocurrent density is ≈13.9 mA cm^{-2}, which corresponds to a power conversion efficiency of 6.0%.

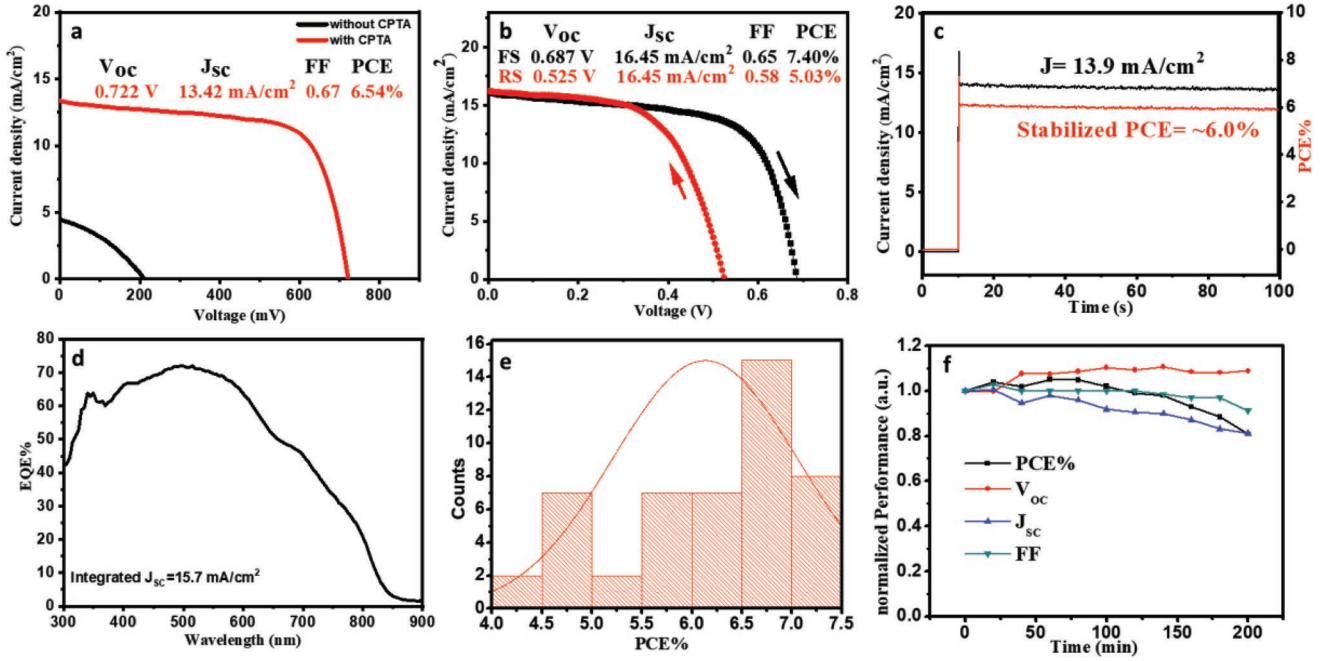

Figure 3. Photovoltaic performance of the {en}$FASnI_3$ solar cells. a) *J–V* scan under simulated AM1.5 sunlight for a solar cell (forward scan, relative humidity = 60%, RT = 25 °C). Black line, without CPTA; red line, with CPTA. b) *J–V* curves of the champion device measured using both forward and reverse scan. The V_{oc} is 0.687 and 0.525 V for forward scan and reverse scan respectively (50 mV s^{-1} scanning rate). c) Stabilized photocurrent output of the solar cell under bias of 0.435 V. The photocurrent density is ≈13.9 mA cm^{-2}, which corresponds to a power conversion efficiency of 6.0%. d) The EQE curve of the solar cell, and the integrate current density is 15.7 mA cm^{-2}. e) Histograms of PCEs for 48 PSCs. f) Device performance of the solar cell stored in ambient air without encapsulation for 200 min (60% humidity, T = 25 °C).

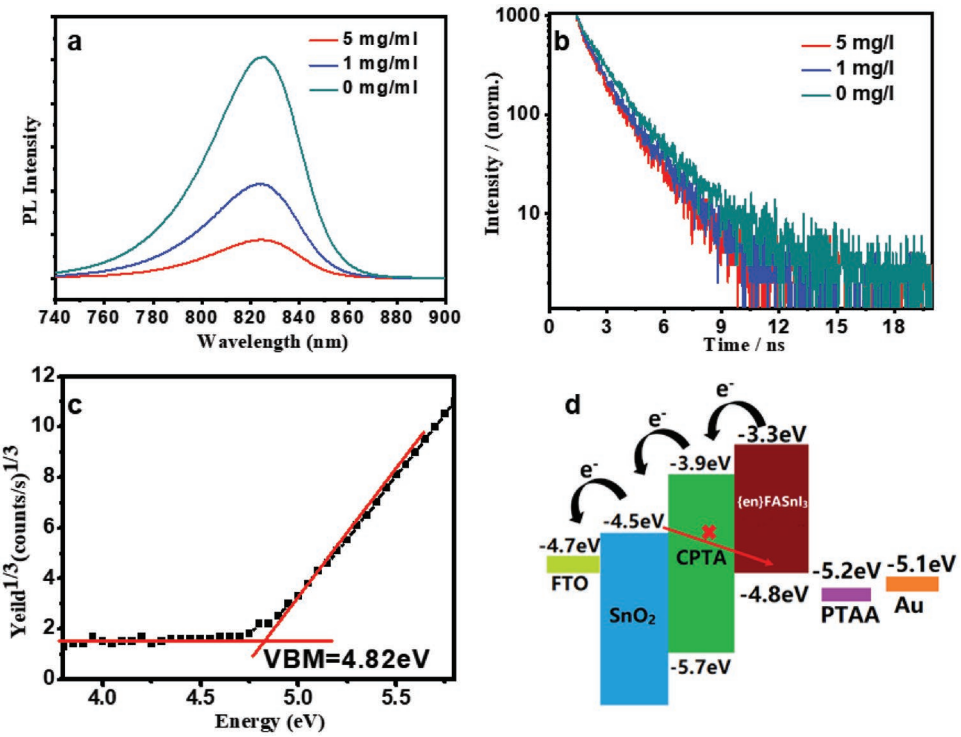

Figure 4. a) Photoluminescence spectra b) time-resolved photoluminescence spectra (excitation wavelength: 479 nm) of the {en}$FASnI_3$ films. c) Photoemission spectroscopy measurements of {en}$FASnI_3$ films deposited on FTO/SnO_2/CPTA substrates. According to the theories of photoelectric emission from semiconductors, the relationship between the photon energy and the cube root of the photoelectron yields gives a linear line (the cubic law).[38] The intersection of the ground level line and the regression line, corresponds to a VBM of –4.82 eV. d) Energy band alignment diagram of the Sn-based PSCs. The energy position of Sn based perovskite is taken from Figure 3c, and the energy positions for other layers are taken from literatures.[17,39] The red arrow illustrates the recombination at the SnO_2/{en}$FASnI_3$ interface.

The photocurrent density can be stabilized almost 100 s, even though the measurement is under an ambient condition (relative humidity = 60%, RT = 25 °C). The J_{SC} integrated from the EQE curves of the PSC is 15.7 mA cm^{-2}, in agreement with the J_{SC} obtained from the *J*–*V* measurement (Figure 3d). We also fabricated 48 devices in several batches to testify the reproducibility of our devices, as depicted in Figure 3e. Most of the devices had more than 6% efficiency, revealing a good reproducibility of our device fabrication. The devices fabricated by our method were highly air-stable (Figure 3f). The devices without encapsulation were stored under ambient condition (60–70% humidity, T = 25 °C), and the *J*–*V* curves were measured every 20 min (forward scan). After 200 min, the PCE is still 80% of the initial efficiency. In the first 60 min, the PCE of the newly fabricated cell did not decrease, but slightly increased, due to the slight increase of the open circuit voltage.[12] The decrease of device efficiency is mainly caused by short circuit current density and fill factor. Figure S6 in the Supporting Information shows the stability of PSCs without encapsulation in a N_2-filled glove box. The un-encapsulated PSCs were still measured under ambient air condition. After we placed the device in the glove box for 100 h, the PCE kept the initial efficiency of 88%.

In order to study the effects of CPTA layer on the electron transfer, photoluminescence (PL) and time-resolved photoluminescence (TRPL) technique were employed to investigate the {en}$FASnI_3$ perovskite films grown on SnO_2 and SnO_2-CPTA. As the thickness of the CPTA layer increases, the fluorescence quenching goes to a high degree (**Figure 4**a). Since the crystal quality of both substrates is similar on different substrates (Figure S7, Supporting Information), the quenching indicates that SnO_2-CPTA is more effective for charge separation than SnO_2.[40] In addition, the perovskite film grown on SnO_2 exhibited a PL decay lifetime τ of 1.5 ns, whereas the lifetime was gradually reduced to 1.2 ns on the SnO_2-CPTA substrate (Figure 4b), showing a faster electron transfer process. Photoemission spectroscopy is further adopted to characterize the electronic structure of {en}$FASnI_3$ (Figure 4c). The valence band maxima (VBM) of the {en}$FASnI_3$ (10% amount of en) is determined to be –4.8 eV, deduced from their ionization potentials. Also, the VBM of {en}$FASnI_3$ achieved by ultraviolet photoelectron spectroscopy (UPS) is consistent with the result (Figure S8, Supporting Information). Together with the optical bandgap,[15] the CBM was calculated to be –3.3 eV. The valence band maxima (VBM) and conduction band minima (CBM) of each functional layer are summarized in Figure 4d.[17,39] The CBM of CPTA (–3.9 eV) is obviously much higher than the CBM of SnO_2 (–4.5 eV), which reduces the energy loss during the electron transfer across the SnO_2/{en}$FASnI_3$ interface when CPTA is present. More importantly, we note that the CBM of SnO_2 (–4.5 eV) is close to the VBM of {en}$FASnI_3$ (–4.8 eV). The electrons transferred to SnO_2 might be prone to recombine with the photogenerated holes inside perovskite layer, causing low V_{OC} for the devices. In other words, SnO_2 layer will not be effective for hole blocking in the

{en}$FASnI_3$ solar cells, though it might be effective for the electron transport.

We note that the VBM is positioned around –4.8 eV for Sn-based perovskites ($FASnI_3$, $MASnI_3$, etc.),[12,17,35] and it might be generalized that the electrons transferred to SnO_2 will recombine with the holes in Sn-perovskites and thus causes low V_{OC}. For this reason, SnO_2, an electron transport layer commonly used in lead-based perovskites, is no longer suitable for tin-based perovskites. We believe that this is why there were no successful examples for preparing Sn-based PSCs on SnO_2. In contrast, the energy barrier at the SnO_2/CPTA interface would effectively suppress charge recombination (block the holes). Therefore, the CPTA layer introduced here is essential for the success in fabricating efficient {en}$FASnI_3$ solar cells. We also note that although the VBM of {en}$FASnI_3$ is slightly higher than that of the PTAA, the surface of the Sn-based perovskite films is p-doped,[6,18,27] producing an Ohmic contact with the PTAA layer. We also substitute SnO_2-CPTA for SnO_2-$PC_{61}BM$ as the electron transport layer. However, the performances of the PSCs are poor (Figure S9, Supporting Information). One of the differences is that the wettability of perovskite precursor solution on the surface of $PC_{61}BM$ is worse than that on the surface of CPTA (Figure S10, Supporting Information). Moreover, the μ_e of CPTA (5.4×10^{-3} cm^2 V^{-1} s^{-1}) is twice as high as that of $PC_{61}BM$ (2.1×10^{-3} cm^2 V^{-1} s^{-1}).[39,40]

3. Conclusion

To summarize, we have successfully fabricated high-quality {en}$FASnI_3$ films after systematic optimizing of the antisolvent assisted one-step method. SnO_2, an electron transport layer commonly used in lead-based perovskite, is found to be problematic for tin-based perovskite. After introduction of CPTA-modified SnO_2 film as the electron selective contact, we have achieved a power conversion efficiency of 7.40% with planar structured {en}$FASnI_3$ solar cells of the normal n–i–p architecture. A record high V_{oc} of 0.72 V is obtained for {en}$FASnI_3$ solar cells. Our research clarifies the confusions on {en}$FASnI_3$ solar cells and demonstrates the feasibility of highly-efficient Sn-based perovskite for solar cell applications. This will help to establish a robust platform to research for further optimization and elucidation of the detailed working mechanisms.

4. Experimental Section

FAI and PTAA were purchased from Xi'an Polymer Technology Co. (China). The SnO_2 colloid solution (tin(IV) oxide, 15% in H_2O colloidal dispersion) was purchased from Alfa Aesar. SnI_2 and CPTA were purchased from Sigma-Aldrich. The chloroform was purchased from J&K Scientific Ltd. (China).

CPTA/$PC_{61}BM$ Solution: Different concentrations (0, 1, 5 mg mL) of CPTA were dissolved in 1.0 mL DMF; for PCBM solution, 5 mg $PC_{61}BM$ was dissolved in 1 mL chlorobenzene.

Perovskite Precursor Solution: 0.408 g of SnI_2, 0.032 g enI_2, and 0.172 g FAI were dissolved in a mixture of DMF (0.5 mL) and DMSO (0.3 mL). Similar to the literature,[15] 0.024 g SnF_2 was added to relieve the detrimental effects from the presence of Sn^{4+}.[10] The solution was filtered before use through a 0.22 µm filter.

HTM Solution: 32 mg PTAA (poly[bis(4-phenyl)(2,4,6-trimethylphenyl) amine], M_W = 15 000-50 000) and 3.6 mg 4-Isopropyl-4′-methyldiphenyliodonium tetrakis(pentafluorophenyl) borate (TCI) was dissolved into chlorobenzene (1.6 mL). After stirring for 30 min, the solution was filtered before use through a 0.22 µm filter.

ETM Solution: The SnO_2 colloid precursor solution (tin (IV) oxide, 15% wt in H_2O colloidal dispersion) was diluted to 2.5% wt. LiCl was added to the ETM solution (0.01 mmol mL^{-1}). The diluted solution was stirred for 30 min right before being spin coated.

FTO glass (15 Ω per square, OPV tech Co., China) was used as the transparent conductive substrate for device fabrication. The substrates (1.5 cm × 1.5 cm in dimension) were sequentially cleaned via ultrasonication in aqueous detergent solution, deionized water, and isopropanol. The solvent-cleaned substrates were then treated with oxygen plasma for 6 min. For SnO_2 layer fabrication, the SnO_2 precursor solution was spin-coated onto the substrate at 4000 rpm for 30 s, and then the SnO_2 covered substrates were annealed at 150 °C for 30 min. After that, the substrates were transferred to a N_2-filled glove box. The CPTA solution was spin-coated onto the SnO_2-covered FTO substrate at 2000 rpm for 30 s, and the substrates were then annealed at 80 °C for 30 min.

The {en}$FASnI_3$ films were then fabricated through a one-step method assisted with antisolvents. After stirring the perovskite precursor solution for 20 min, the precursor solution was spin-coated onto SnO_2-covered FTO substrates at 3000 rpm for 1 min. At the late stage, 0.5 mL chloroform was poured onto the substrate. After a following heating process at 110 °C for 15 min, the precursor films transformed into the desired {en}$FASnI_3$ films.

The perovskite solar cells were fabricated in a normal device configuration: FTO/SnO_2/CPTA/{en}$FASnI_3$/PTAA/Au. PTAA was spin coated onto {en}$FASnI_3$ films as the hole-transport layer at 1500 rpm for 30 s and annealed at 70 °C for 5 min. Finally, 80 nm Au layer was then deposited on top of PTAA for the collection of the carriers. After PTAA was deposited, the {en}$FASnI_3$ samples were taken out of the glove box, and quickly (≈10 min) got transferred to an evaporator for Au deposition.

The photovoltaic characterization of the un-encapsulated {en}$FASnI_3$ devices was carried out under the ambient conditions in the laboratory. A Newport Sol3A solar simulator was used as the sunlight source, and the light intensity was calibrated (100 mW cm^{-2}) with a standard Si solar cell available from Newport. A Keithley 2400 was used to bias the solar cells and to collect the current signal. The active area of the device was 0.1 cm^2, which was defined by a metal mask. The incident photon-to-current Efficiency (IPCE) spectra of the devices were collected via a Crowntech IPCE system.

A PANalytical high resolution PXRD (Cu target, line, 1.5406 Å) was used for the X-ray characterization of the perovskite films. The scanning rate was set at 4° per min and the step size was 0.02°. UV–vis absorption spectra of the planar perovskite films were characterized by an UV/Vis spectrophotometer (Hitachi U-4100). SEM images of perovskite films were characterized via a field emission scanning electron microscopy (Hitachi S4800). The thickness of CPTA layer was measured via an atomic force microscope (Bruker Dimension Icon). The steady state photoluminescence (PL) spectra of the {en}$FASnI_3$ films were collected via a NanoLog infrared fluorescence spectrometer (Nanolog FL3-2iHR). Time resolved fluorescence of {en} $FASnI_3$ films was collected via an UltraFast lifetime Spectrofluorometer Delta flex. A Hamamatsu 479 nm diode laser was used as the excitation source. The ^1H NMR spectra of films were recorded on a Bruker-500 MHz NMR (AVANCE III). XPS was carried out using an Imaging X-ray photoelectron spectrometer (Axis Ultra). Photoemission spectroscopy measurements were carried out using a photoelectron spectrometer (AC-2). Ultraviolet photoelectron spectroscopy (UPS) spectra was measured by an imaging photoelectron spectrometer (ESCALAB250Xi, ThermoFisher Scientific Ltd), with a non-monochromated He I photon source ($h\nu$ = 21.11 eV). Raman spectra were measured on a Raman microscope (Horiba-Jobin Yvon system) with a wavelength ranging from 100 to 3000 cm^{-1}.

Supporting Information

Supporting Information is available from the Wiley Online Library or from the author.

Acknowledgements

This work was supported by the National Natural Science Foundation of China (Grant No. 21821004) and the National Basic Research Program of China (No. 2014CB239303). The authors thank Dr. Y. Guan, M. Chen, W. Pan (Analytical Instrumentation Center, Peking University) for their help in the measurement of Nanolog FL3-2iHR and AC-2.

Conflict of Interest

The authors declare no conflict of interest.

Keywords

CPTA-modified SnO_2, $FASnI_3$, hybrid perovskite solar cells, planar structure

Received: May 6, 2019
Revised: July 1, 2019
Published online: August 12, 2019

[1] A. Kojima, K. Teshima, Y. Shirai, T. Miyasaka, *J. Am. Chem. Soc.* **2009**, *131*, 6050.
[2] NREL, Best Research-Cell Efficiencies, https://www.nrel.gov/pv/cell-efficiency.html (accessed: April 2019).
[3] B. Hailegnaw, S. Kirmayer, E. Edri, G. Hodes, D. Cahen, *J. Phys. Chem. Lett.* **2015**, *6*, 1543.
[4] F. Hao, C. C. Stoumpos, D. H. Cao, R. P. H. Chang, M. G. Kanatzidis, *Nat. Photonics* **2014**, *8*, 489.
[5] N. K. Noel, S. D. Stranks, A. Abate, C. Wehrenfennig, S. Guarnera, A.-A. Haghighirad, A. Sadhanala, G. E. Eperon, S. K. Pathak, M. B. Johnston, A. Petrozza, L. M. Herz, H. J. Snaith, *Energy Environ. Sci.* **2014**, *7*, 3061.
[6] C. C. Stoumpos, C. D. Malliakas, M. G. Kanatzidis, *Inorg. Chem.* **2013**, *52*, 9019.
[7] M. Konstantakou, T. Stergiopoulos, *J. Mater. Chem. A* **2017**, *5*, 11518.
[8] F. Gu, S. Ye, Z. Zhao, H. Rao, Z. Liu, Z. Bian, C. Huang, *Sol. RRL* **2018**, *2*, 1800136.
[9] Y. Takahashi, H. Hasegawa, Y. Takahashi, T. Inabe, *J. Solid State Chem.* **2013**, *205*, 39.
[10] M. H. Kumar, S. Dharani, W. L. Leong, P. P. Boix, R. R. Prabhakar, T. Baikie, C. Shi, H. Ding, R. Ramesh, M. Asta, M. Gratzel, S. G. Mhaisalkar, N. Mathews, *Adv. Mater.* **2014**, *26*, 7122.
[11] T. B. Song, T. Yokoyama, C. C. Stoumpos, J. Logsdon, D. H. Cao, M. R. Wasielewski, S. Aramaki, M. G. Kanatzidis, *J. Am. Chem. Soc.* **2017**, *139*, 836.
[12] E. Jokar, C. H. Chien, C. M. Tsai, A. Fathi, E. W. Diau, *Adv. Mater.* **2019**, *31*, 1804835.
[13] S. Shao, J. Liu, G. Portale, H.-H. Fang, G. R. Blake, G. H. ten Brink, L. J. A. Koster, M. A. Loi, *Adv. Energy Mater.* **2018**, *8*, 1702019.
[14] W. Ke, P. Priyanka, S. Vegiraju, C. C. Stoumpos, I. Spanopoulos, C. M. M. Soe, T. J. Marks, M. C. Chen, M. G. Kanatzidis, *J. Am. Chem. Soc.* **2018**, *140*, 388.
[15] W. Ke, C. C. Stoumpos, M. Zhu, L. Mao, I. Spanopoulos, J. Liu, O. Y. Kontsevoi, M. Chen, D. Sarma, Y. Zhang, M. R. Wasielewski, M. G. Kanatzidis, *Sci. Adv.* **2017**, *3*, e1701293.
[16] W. Ke, C. C. Stoumpos, I. Spanopoulos, L. Mao, M. Chen, M. R. Wasielewski, M. G. Kanatzidis, *J. Am. Chem. Soc.* **2017**, *139*, 14800.
[17] W. Ke, C. C. Stoumpos, M. G. Kanatzidis, *Adv. Mater.* **2018**, 1803230.
[18] W. Ke, C. C. Stoumpos, J. L. Logsdon, M. R. Wasielewski, Y. Yan, G. Fang, M. G. Kanatzidis, *J. Am. Chem. Soc.* **2016**, *138*, 14998.
[19] L. Liang, P. Gao, *Adv. Sci.* **2018**, *5*, 1700331.
[20] K.-H. Jung, J.-Y. Seo, S. Lee, H. Shin, N.-G. Park, *J. Mater. Chem. A* **2017**, *5*, 24790.
[21] D. Yang, R. Yang, K. Wang, C. Wu, X. Zhu, J. Feng, X. Ren, G. Fang, S. Priya, S. Liu, *Nat. Commun.* **2018**, *9*, 3239.
[22] T. Salim, S. Sun, Y. Abe, A. Krishna, A. C. Grimsdale, Y. M. Lam, *J. Mater. Chem. A* **2015**, *3*, 8943.
[23] N. Wang, Y. Zhou, M.-G. Ju, H. F. Garces, T. Ding, S. Pang, X. Zeng, N. P. Padture, X. Sun, *Adv. Energy Mater.* **2016**, *6*, 1601130.
[24] Z. Zhu, C. C. Chueh, N. Li, C. Mao, A. K. Jen, *Adv. Mater.* **2018**, *30*, 1703800.
[25] S. Gupta, D. Chen, G. Hodes, *J. Phys. Chem. C* **2018**, *122*, 13926.
[26] F. Hao, C. C. Stoumpos, P. Guo, N. Zhou, T. J. Marks, R. P. Chang, M. G. Kanatzidis, *J. Am. Chem. Soc.* **2015**, *137*, 11445.
[27] T. Yokoyama, D. H. Cao, C. C. Stoumpos, T.-B. Song, Y. Sato, S. Aramaki, M. G. Kanatzidis, *J. Phys. Chem. Lett.* **2016**, *7*, 776.
[28] F. Li, C. Zhang, J. Huang, H. Fan, H. Wang, P. Wang, C. Zhan, C. Liu, X. Li, L. Yang, Y. Song, K. Jiang, *Angew. Chem., Int. Ed.* **2019**, *58*, 6688.
[29] S. J. Lee, S. S. Shin, Y. C. Kim, D. Kim, T. K. Ahn, J. H. Noh, J. Seo, S. I. Seok, *J. Am. Chem. Soc.* **2016**, *138*, 3974.
[30] J. Liu, M. Ozaki, S. Yakumaru, T. Handa, R. Nishikubo, Y. Kanemitsu, A. Saeki, Y. Murata, R. Murdey, A. Wakamiya, *Angew. Chem., Int. Ed.* **2018**, *57*, 13221.
[31] Y. Wang, Y. Liang, Y. Zhang, W. Yang, L. Sun, D. Xu, *Adv. Funct. Mater.* **2018**, *28*, 1801237.
[32] L. Ma, F. Hao, C. C. Stoumpos, B. T. Phelan, M. R. Wasielewski, M. G. Kanatzidis, *J. Am. Chem. Soc.* **2016**, *138*, 14750.
[33] W. Liao, D. Zhao, Y. Yu, C. R. Grice, C. Wang, A. J. Cimaroli, P. Schulz, W. Meng, K. Zhu, R.-G. Xiong, Y. Yan, *Adv. Mater.* **2016**, *28*, 9333.
[34] R. Hu, Y. Ouyang, T. Liang, H. Wang, J. Liu, J. Chen, C. Yang, L. Yang, M. Zhu, *Adv. Mater.* **2017**, *29*, 1605006.
[35] Z. Zhao, F. Gu, Y. Li, W. Sun, S. Ye, H. Rao, Z. Liu, Z. Bian, C. Huang, *Adv. Sci.* **2017**, *4*, 1700204.
[36] I. Levine, P. K. Nayak, J. T.-W. Wang, N. Sakai, S. Van Reenen, T. M. Brenner, S. Mukhopadhyay, H. J. Snaith, G. Hodes, D. Cahen, *J. Phys. Chem. C* **2016**, *120*, 16399.
[37] Y. Yuan, J. Huang, *Acc. Chem. Res.* **2016**, *49*, 286.
[38] J. M. Ballantyne, *Phys. Rev. B* **1972**, *6*, 1436.
[39] Y.-C. Wang, X. Li, L. Zhu, X. Liu, W. Zhang, J. Fang, *Adv. Energy Mater.* **2017**, *7*, 1701144.
[40] P. Docampo, J. M. Ball, M. Darwich, G. E. Eperon, H. J. Snaith, *Nat. Commun.* **2013**, *4*, 2761.